AGU PUBLICATIONS

JGR

Journal of Geophysical Research: Space Physics

RESEARCH ARTICLE
10.1002/2015JA021639

Key Points:
- GPS receiver biases demonstrate true seasonal variability
- True receiver bias variability appears to be driven by temperature variability
- Technique assumptions result in errors of up to 10 TECU in the polar cap region

Correspondence to:
D. R. Themens,
david.themens@gmail.com

Citation:
Themens, D. R., P. T. Jayachandran, and R. B. Langley (2015), The nature of GPS differential receiver bias variability: An examination in the polar cap region, *J. Geophys. Res. Space Physics*, *120*, 8155–8175, doi:10.1002/2015JA021639.

Received 1 JUL 2015
Accepted 28 AUG 2015
Accepted article online 3 SEP 2015
Published online 30 SEP 2015

The nature of GPS differential receiver bias variability: An examination in the polar cap region

David R. Themens[1], P. T. Jayachandran[1], and Richard B. Langley[2]

[1]Department of Physics, University of New Brunswick, Fredericton, New Brunswick, Canada, [2]Department of Geodesy and Geomatics Engineering, University of New Brunswick, Fredericton, New Brunswick, Canada

Abstract While modern GPS receiver differential code bias estimation techniques have become highly refined, they still demonstrate unphysical behavior, namely, notable solar cycle variability. This study investigates the nature of these seasonal and solar cycle bias variabilities in the polar cap region using single-station bias estimation methods. It is shown that the minimization of standard deviation bias estimation technique is linearly dependent on the user's choice of shell height, where the sensitivity of this dependence varies significantly from 1 total electron content unit (1 TECU = 10^{16} el m^{-2}) per 4000 km in solar minimum winter to in excess of 1 TECU per 90 km during solar maximum summer. Using an ionosonde, we find appreciable shell height variability resulting in bias variabilities of up to 2 TECU. Comparing northward face Resolute Incoherent Scatter Radar (RISR-N) measurements to a collocated GPS station, we find that RISR-derived GPS receiver biases vary seasonally but not with solar cycle. RMS differences between bias estimation methods and observation between 2009 and 2013 were found to range from 2.7 TECU to 3.4 TECU, depending on method. To account for the erroneous solar cycle variability of standard bias estimation approaches, we linearly fit these biases to sunspot number, removing the trend. RMS errors after sunspot detrending these biases are reduced to 1.91 TECU. Also, these ISR-derived and sunspot-detrended biases are fit to ambient temperature, where a significant correlation is found. By using these temperature-fitted biases we further reduce RMS errors to 1.66 TECU. These results can be taken as further evidence of temperature-dependent dispersion in the GPS cabling and antenna hardware.

1. Introduction

The Global Positioning System (GPS) has become an important source of ionospheric observations; however, in order to provide accurate ionospheric information, GPS measurements must be calibrated to account for both receiver and satellite biases [*Warnant*, 1997; *Rideout and Coster*, 2006]. While several techniques exist for determining these biases, one must take care in their application in regions outside their initial design [*Lanyi and Roth*, 1988; *Ma and Maruyama*, 2003; *Ma et al*., 2005; *Rideout and Coster*, 2006; *Arikan et al*., 2008]. Recent studies have attempted to characterize variabilities in these biases estimated through single-station approaches using real data and simulations [*Ciraolo et al*., 2007; *Mazzella*, 2009; *Zhang et al*., 2009; *Brunini and Azpilicueta*, 2010; *Zhang et al*., 2010; *Conte et al*., 2011; *Coster et al*., 2013]. These studies highlight the need to understand not only the nature of true bias variability but also the impact of the fundamental assumptions made in standard bias estimation techniques on bias estimation.

GPS is capable of measuring total electron content (TEC), the total number of electrons in a meter-squared column centered about the GPS raypath, through the impact of the ionosphere on the system's two legacy radio frequency signals, L1 at 1575.42 MHz and L2 at 1227.60 MHz; namely, the difference in the GPS phase advance or code delay measured on each frequency allows for the calculation of TEC. Details on the process of converting these observables to TEC can be found readily in any one of a number of publications, including *Leick* [2004] or *Themens et al*. [2013]. Within the GPS measurements of TEC, there reside biases due to the satellite and receiver hardware. Satellite biases are regularly calculated by network methods, such as those provided by the University of Bern at ftp.unibe.ch/aiub/; however, receiver biases remain the responsibility of receiver or network operators.

There are several different means of determining GPS receiver biases, all of which are expected to demonstrate appreciable errors in their application to the high-latitude region. *Themens et al*. [2013] showed that the least squares (LSQ) receiver bias estimation method of *Lanyi and Roth* [1988] is highly unstable in its

application to the high-latitude region while used in the same manner as used at midlatitudes. The minimization of standard deviation (MSD) method of *Ma and Maruyama* [2003] is also shown to demonstrate appreciable errors while applied in the polar cap region; however, these errors were found to be far less significant than those of the LSQ method [*Themens et al*., 2013]. While the LSQ and MSD methods can be considered bias-projection-based estimation methods, other methods generally use an ionospheric reference model to estimate biases [*Arikan et al*., 2008; *Keshin*, 2012]. In midlatitude regions, where accurate ionospheric models, such as the International Reference Ionosphere (IRI) and IONospheric EXchange (IONEX) ionospheric maps, are available, reference-based methods demonstrate good performance [*Arikan et al*., 2008]. In high-latitude regions, however, *Themens et al*. [2013] demonstrate that the IONEX maps suffer significant errors due to a lack of contributing data from these regions, and *Themens et al*. [2014] show that there are appreciable errors in the IRI-2007's representation of the polar cap ionosphere. The lack of adequate reference data in this region makes it necessary for operators to explore alternative receiver bias estimation approaches for application in the high-latitude region. It should be noted that receiver biases provided by sources, such as the University of Bern, or calculated using any of the above receiver bias estimation techniques generally refer not only to the bias of the receiver itself but also to biases potentially produced by the antenna hardware or cabling.

This study examines the behavior of standard, single-station, receiver bias estimation techniques (MSD and LSQ methods), specifically in their application to the polar cap region. Based on this assessment we make recommendations for their modification to account for limitations specific to high-latitude regions, some of which are outlined by *Themens et al*. [2013]. The data sources used in this study, including GPS, ionosonde, and incoherent scatter radar (ISR), are presented in section 2. Section 3 examines the methodology and assumptions of the MSD and LSQ bias estimation methods. Finally, results are examined in section 4, where we evaluate the performance of these bias estimation techniques in their application to the polar cap region.

2. Data

In this study, we make use of several remote sensing instruments in an attempt to determine the true GPS receiver bias and assess the performance of common GPS receiver bias estimation techniques. These instruments include Canadian Advanced Digital Ionosondes (CADIs) and GPS systems, operated by the Canadian High Arctic Ionospheric Network (CHAIN), and the Resolute Incoherent Scatter Radar (RISR), operated by SRI International.

2.1. Canadian High Arctic Ionospheric Network

CHAIN operates 21 stations in the Canadian Arctic region. Ten stations are equipped with NovAtel GSV4004B dual-frequency GPS receivers, six of which are collocated with a Canadian Advanced Digital Ionosonde (CADI). The remaining 11 stations are equipped with Septentrio PolaRx PRO receivers. Figure 1 shows the locations of all currently operated CHAIN stations. These GPS systems allow for the accurate estimation of TEC and CADI systems that provide accurate bottomside electron density in the auroral oval and polar cap regions [*Jayachandran et al*., 2009; *Themens et al*., 2013].

2.1.1. GPS

Dual-frequency GPS receivers typically measure two observables on each carrier frequency that are important in TEC calculation, namely, pseudorange and carrier phase. TEC can be considered proportional to the difference between the pseudorange or carrier phase measurements from each signal to the first and second order [*Petrie et al*., 2011]. While both of these differences yield some measure of information about TEC, they each suffer shortcomings, which must be accounted for prior to using these versions of TEC. Pseudorange TEC measurements are accurate but are subject to significant measurement noise and can suffer from multipath errors. Carrier phase TEC measurements, while far more precise and less sensitive to multipath than their pseudorange counterparts, suffer from a cycle ambiguity that must be resolved before their use [*Leick*, 2004].

To take advantage of the favorable properties of each observable, we undertake a process known as phase levelling, which alters the "level" of the carrier phase TEC measurements to that of the pseudorange measurements over each arc of lock [*Dyrud et al*., 2008]. This process can vary depending on data availability/cadence and performance, but the method chosen for the following analysis is that outlined by *Themens et al*. [2013], where the means of the carrier phase and pseudorange TEC from the top 10° of the lock arc are used to level the carrier phase TEC to the pseudorange TEC.

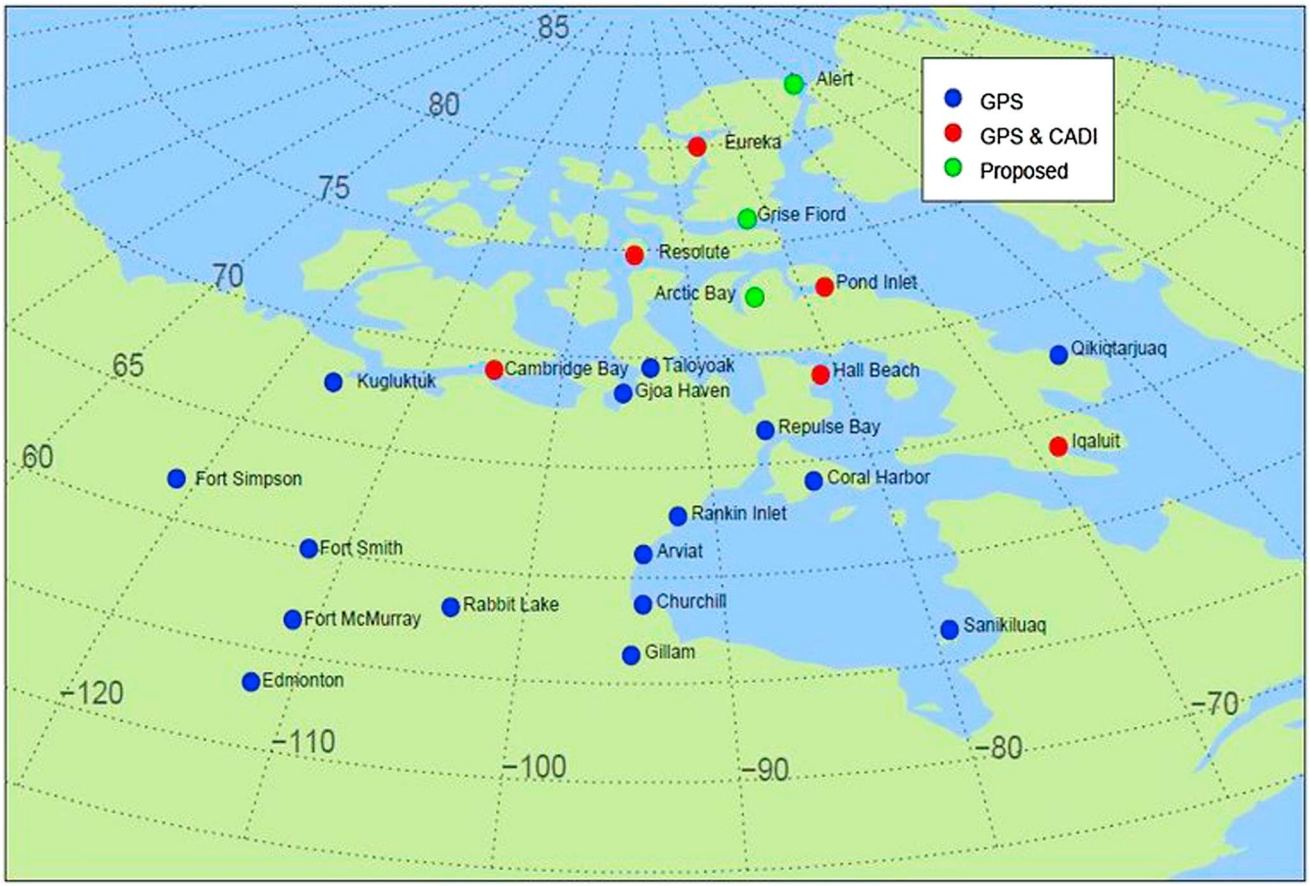

Figure 1. Map of the current CHAIN network stations. GPS stations are marked by blue circles, stations with both GPS and ionosonde systems are marked by red circles, and planned GPS stations are marked by green circles.

In this work, we will often make reference to vertical TEC (vTEC), which is the TEC that would be measured along a vertical path through the ionosphere. As the path length of the GPS signal through the ionosphere is dependent on the elevation angle of the measurement, it is often difficult to compare GPS slant TEC (sTEC) measurements. To remove the geometric dependence of these measurements, sTEC is often projected to vTEC using one of several possible projection functions. In this study, we make use of one of the most common and simple projection functions, which is derived using the Thin Shell Ionosphere Model (TSIM) [*Themens et al.*, 2013]. In this method, we assume that the ionosphere can be represented by an infinitesimally thin and horizontally homogeneous shell about the Earth. Under this assumption, the TEC along a vertical path passing through the intercept between the slant GPS raypath and the thin shell, called the Ionospheric Pierce Point (IPP), can be calculated as

$$\mathrm{vTEC} = \mathrm{sTEC} \cdot M(e) \tag{1}$$

$$M(e) = \cos(\chi) = \sqrt{1 - \left(\frac{R\cos(e)}{R+h}\right)^2} \tag{2}$$

where h is an assumed height of the ionosphere (taken here as 400 km), R is the radius of the Earth, e is the elevation angle of the satellite raypath, and sTEC is the TEC measured along the slant GPS raypath [*Gaussiran et al.*, 2004]. GPS receiver biases must be removed prior to the projection of sTEC to vTEC, as receiver biases are not dependent on the geometric configuration of the system and should not be projected.

2.1.2. CADI

In this study, we use CADI-derived electron density profiles to estimate the ionospheric structure and height for comparison with the assumed ionospheric structure used in GPS vTEC calculation and to act as a simulation environment for assessing the behavior of GPS receiver bias estimation techniques.

CADI, a modern digital ionosonde, produces ionograms (frequency-height profiles of ionospheric critical frequencies and associated virtual heights) by sweeping through a frequency range from 1 to 20 MHz while timing echo signals reflected from the ionosphere [*Themens et al*., 2013]. These critical frequencies are directly related to the electron density at the location of reflection and can be retrieved up to the height of the ionosphere's peak electron density [*Davies*, 1990]. These virtual height profiles are then inverted to true height electron density profiles through the use of the Polynomial Analysis (POLAN) method with manually scaled virtual height profiles as input [*Titheridge*, 1985, 1988]. Ionograms are available in either 1 or 5 min temporal resolution and 6 km altitude resolution from the CHAIN network, depending on the station and time of study (all data after the summer of 2009 are at 1 min temporal resolution). To get topside electron density, we use the NeQuick topside model of *Coïsson et al*. [2006] to extrapolate the density profile up to 2000 km altitude.

2.2. Resolute Incoherent Scatter Radar

ISRs are powerful tools for observing the ionosphere. Based on the theory of *Evans* [1969], incoherent scatter radars are capable of providing full electron density profiles of the ionosphere. The northward looking face of the RISR (RISR-N) is a deployment of the Advanced Modular ISR class of phased array ISR systems and is located in Resolute, Canada (74.73°N, 265.09°E), which is within a few kilometers of the CHAIN Resolute station. It provides electron density profiles along several beam directions to a maximum range of approximately 700 km for long-pulse (LP) operation or approximately 400 km for alternating code (AC) operation. System details may be found in *Bahcivan et al*. [2010]. Details about the calibration and accuracy of the RISR-N can be found in *Themens et al*. [2014].

In this study, measurements from the RISR-N are compared to GPS sTEC measurements in an attempt to identify the nature of GPS bias variability. To undertake this comparison, we first processed the ISR data into a more manageable form by binning all data from all available beams over 5 min intervals into 5 km thick vertical bins and taking the mean of each bin. A 5 min interval was chosen to ensure that, when both AC and LP modes are run in an alternating fashion (a standard operation of the RISR-N system), each interval contains at least one set of both AC and LP measurements, ensuring some consistency in observation region between intervals. To account for the limited range of the ISR, the resulting electron density profiles were least squares fit to the NeQuick topside model and extrapolated to 2000 km altitude [*Coïsson et al*., 2006]. An example of the RISR-N beam pattern for 22 November 2010 is presented in Figure 2.

2.3. GPS Simulation

In this study, we employ a simple, idealized simulation, where the vertical structure of the ionosphere is derived from the Resolute ionosonde and the ionosphere is simulated as horizontally homogeneous; thus, this simulation upholds the horizontal homogeneity assumption of the TSIM projection. To afford some realism, we first determined the satellite coordinates (azimuth and elevation) as seen by the Resolute location. Once these were identified, sTEC was calculated for each satellite in view by analytically determining the sTEC through each layer of the simulated ionosphere and integrating along the raypath. The 10 km thick layers between 90 km and 2000 km were chosen for this purpose. Mathematically, the sTEC of each layer is represented by the following relationship:

$$\mathrm{sTEC}_i = N_i \cdot \left[\sqrt{\left(r_i + \frac{d}{2}\right)^2 - r_i^2 \sin^2 \chi_i} - \sqrt{\left(r_i - \frac{d}{2}\right)^2 - r_i^2 \sin^2 \chi_i} \right] \tag{3}$$

where N_i is the layer density, r_i is the layer height, d is the layer thickness, and χ_i is the piercing angle of the GPS raypath through the layer [*Smith et al*., 2008]. Once sTEC has been simulated, we add a test bias to the sTEC data and apply the receiver bias estimation method of interest. As a brief test, we have, at times, also added zero-mean Gaussian noise to the simulated sTEC in order to identify the method's behavior in the presence of horizontal inhomogeneity/small-scale gradients or satellite bias errors.

2.4. Shell Height Calculation

Receiver bias estimation methods and vTEC projection using the TSIM require the calculation or assumption of an ionospheric shell height. The appropriate shell height is often unavailable to the user; however, there are several

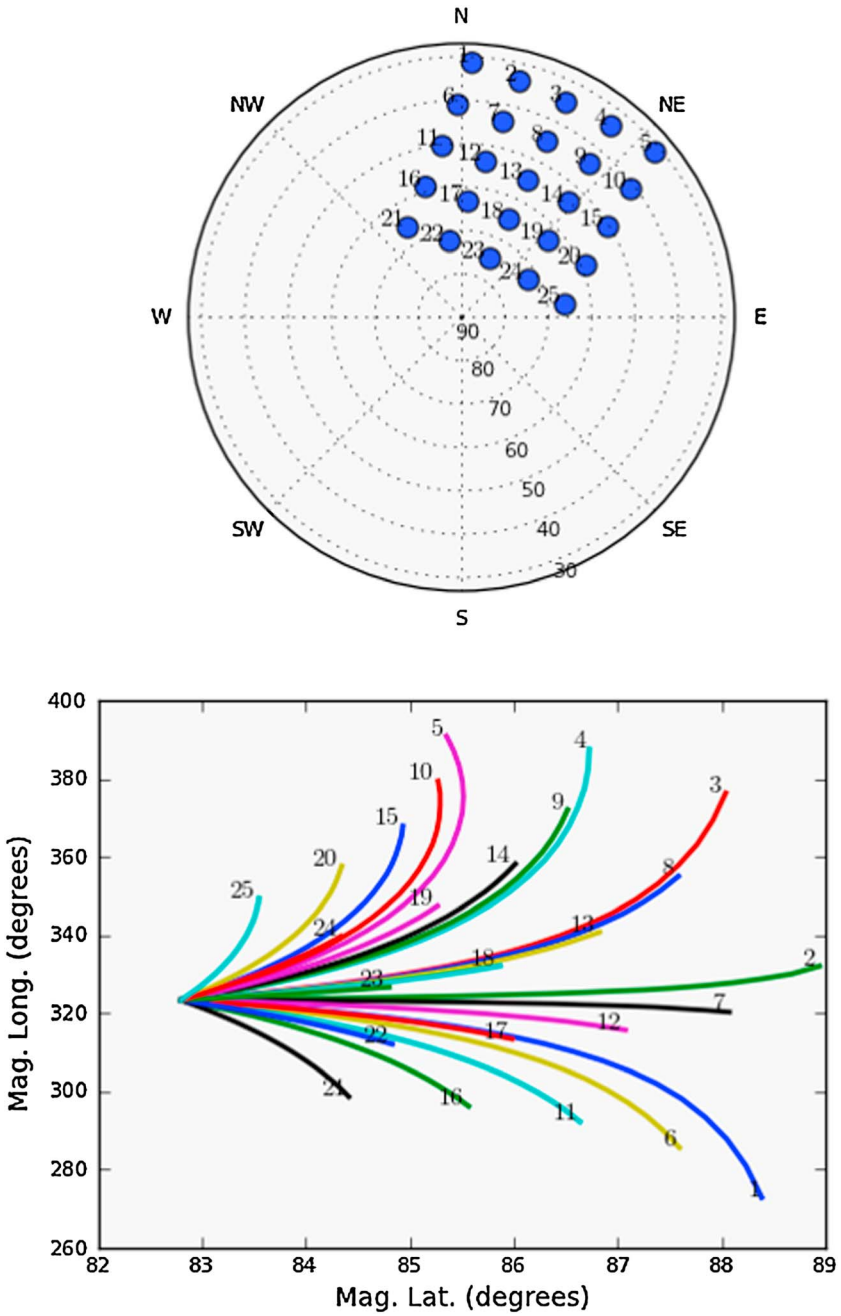

Figure 2. RISR-N beam pattern used on 22 November 2010. (top) Sky plot of beam elevation angles (radius) and azimuths (circumference). (bottom) Ground footprint of beams in geomagnetic coordinates. Numbers correspond to beam number.

methods for calculating it from GPS TEC measurements. The first method requires that a vertical satellite pass be available. In this method, the projection equation can be directly rearranged for shell height such that

$$h = R\left(\frac{\cos e}{\sqrt{1-\left(\frac{\text{vTEC}}{\text{sTEC}}\right)^2}} - 1\right) \tag{4}$$

In the event that there are no vertical satellite passes, which is the case at high latitudes, one may use two slant satellite measurements at different elevations, but with collocated or close IPPs, by equating the expected

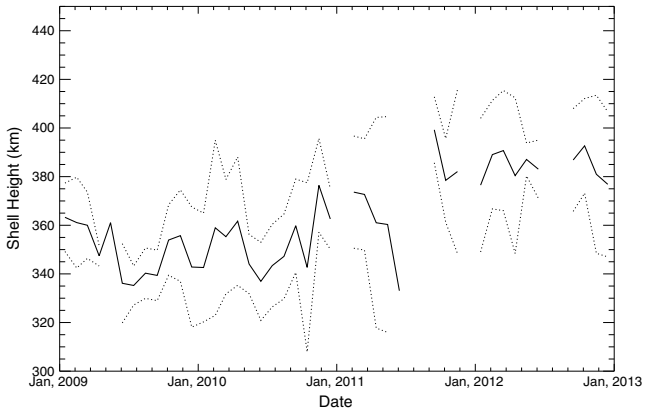

Figure 3. Monthly median shell height (solid) and standard deviation ranges (dashed) at Resolute computed using the CM method with local CADI ionogram data.

vTEC for both satellites (i.e., equating the right-hand side of equation (1) for both satellites) and rearranging into a quadratic equation in h

$$0 = (1 - S)h^2 + 2Rh(1 - S) + R^2\left(\sin^2 e_2 - S \cdot \sin^2 e_1\right) \quad (5)$$

$$S = \left(\frac{\text{sTEC}_1}{\text{sTEC}_2}\right)^2 \quad (6)$$

where subscripts 1 and 2 refer to the first and second satellite of interest. This equation can be simply solved, where the positive root can be taken as the shell height estimate. Both of the above techniques require unbiased TEC to calculate shell height; however, there are approaches to overcome this limitation, such as that of *Birch et al.* [2002]. All of these methods require assumptions on either the horizontal structure or time evolution of the ionosphere, which have not been assessed and may be exacerbated in the dynamic high-latitude ionospheric environment.

Nonetheless, if a vertical electron density profile is available the problem becomes simple. The shell height can be taken as the center of mass (CM) of the profile, as in

$$h = \frac{\int_0^\infty N(z)z dz}{\int_0^\infty N(z)dz} \quad (7)$$

where $N(z)$ is the electron density at altitude z. Monthly median shell height derived using CADI electron density profiles at Resolute using the CM method is presented in Figure 3. As you can see, the standard assumption of 400 km for the a priori shell height in vTEC projection is generally within ~50 km of truth at the Resolute station at solar maximum but should be adjusted to ~350 km for solar minimum conditions. While this error is relatively small, care must be taken to assess its impact on receiver bias estimation.

3. Receiver Bias Estimation Methods

This study makes use of two popular single-station receiver bias estimation methods: namely, MSD and LSQ. These methods, like most single-station bias estimation approaches, rely on three basic assumptions:

1. The ionosphere is locally horizontally homogeneous.
2. The ionosphere can be roughly approximated as a thin spherical shell above the Earth at a specified altitude, or at the very least, the ionosphere can be represented by some standard vertical profile function.
3. The GPS receiver bias is the only geometry/elevation-independent parameter affecting GPS TEC measurements.

While both methods share these assumptions, they do not necessarily behave in the same manner, as each method has some ability to accommodate violations of their fundamental assumptions. In this study, we use a series of simplified simulations and measured data to assess the impact that the method assumptions have on the MSD and LSQ bias approaches.

These approaches to bias estimation are built on the fact that receiver biases are not geometrically dependent properties; thus, when one projects bias-contaminated sTEC to vTEC, one is also erroneously projecting the biases. This leads to elevation-dependent errors in the projected vTEC. Biases can be considered correctly removed when the estimated vTEC no longer contains these erroneous projected biases. This principle is treated slightly differently in each approach pertaining largely to how it is decided that the resulting vTEC no longer contains projected biases.

3.1. Minimization of Standard Deviations

The MSD approach to receiver bias estimation, first proposed by *Ma and Maruyama* [2003], is conceptually one of the simplest approaches to determining receiver biases.

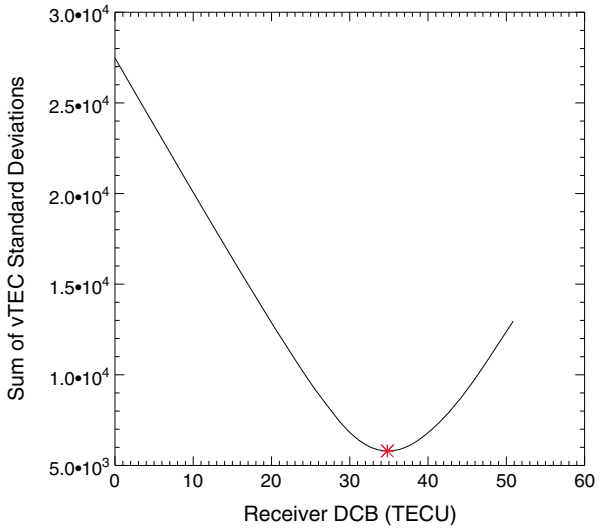

Figure 4. Example of the summed standard deviations versus test bias at Resolute for 24 h integration on 19 September 2009. The minimum summed standard deviation is marked by a red asterisk at the receiver bias value of 34.8 TECU.

3.1.1. Traditional MSD

Let us assume that there are multiple satellites in view at varying elevation angles. The errors resulting from erroneously projecting receiver biases should be different for each satellite measurement; thus, there will be a bias-dependent spread in the derived vTEC values if there are receiver biases in the sTEC measurements. In the MSD approach to bias estimation, it is assumed that, if the bias is correctly removed, this spread in vTEC should be minimized. By iterating through a series of test biases, removed before vTEC projection, and summing the standard deviation of vTEC measurements at each time step, we can identify the correct bias as that which minimizes the summed standard deviations (SSDs). An example of this process is presented in Figure 4, where we have iterated through a series of biases between 0.0 and 50.0 TECU in 0.1 TECU steps over an integration period of 24 h for 19 September 2009, at Resolute. This example demonstrates a clear minimum in summed standard deviations at a bias of 34.8 TECU (marked by a red star). An example of monthly averaged, MSD-calculated biases between January 2009 and August 2013 for the CHAIN Resolute station is presented in Figure 5 using 12 and 24 h integration periods. Daytime bias values are found to be larger than nighttime values by between 1 and 5 TECU, with the 24 h integration biases generally lying between the nighttime and daytime values. Daytime and nighttime periods are chosen as a 12 h period centered about local noon and local midnight, respectively. Biases demonstrate short-term, seasonal, and solar cycle variabilities.

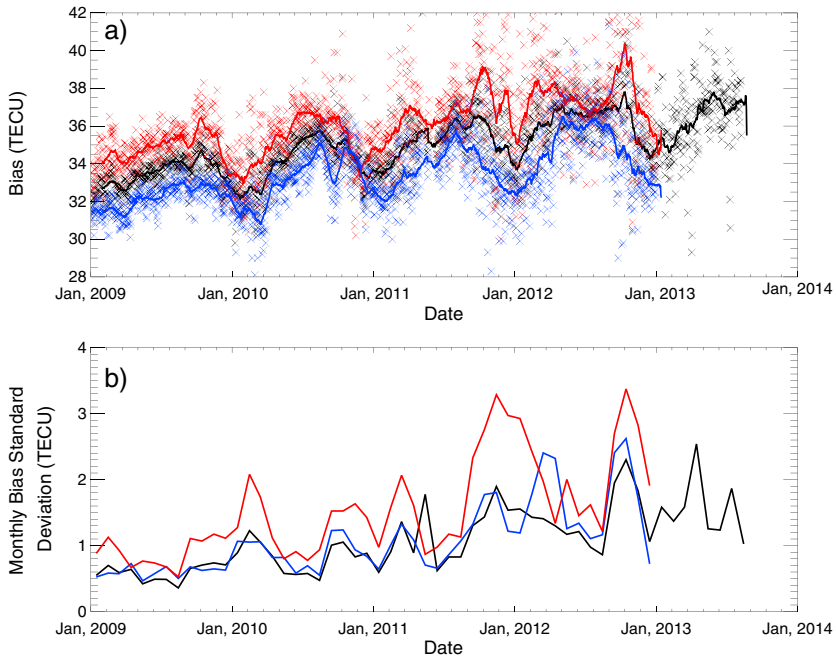

Figure 5. (top) Daytime (red), nighttime (blue), and 24 h (black) MSD biases at Resolute. The 28 day smoothed biases are superimposed as solid lines to simplify interpretation. (bottom) Monthly standard deviation of the biases presented above.

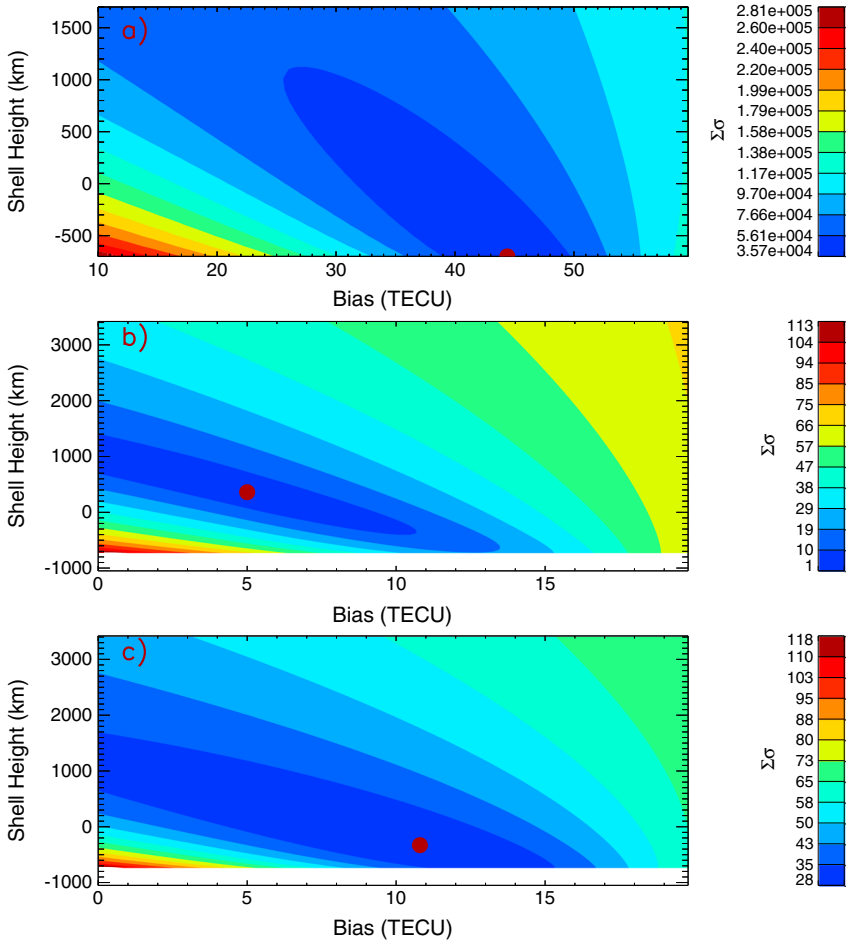

Figure 6. (top) Example of GPS MSD cominimization SSD surface for 1 July 2013, at Resolute. (middle) Example of zero-noise, simulated, MSD cominimization SSD surface for 1 July 2013, at Resolute with 5 TECU simulated bias. (bottom) Example of 1 TECU noise, simulated, MSD cominimization SSD surface for 1 July 2013, at Resolute with 5 TECU simulated bias.

3.1.2. Cominimization

While we have outlined the traditional MSD approach above, we shall briefly take a detour to consider the more fundamental application of the method, namely, where we minimize not only through various test biases but also through various test shell heights. An example of this "cominimization" approach is presented in Figure 6a using 24 h of GPS data from the CHAIN Resolute station, where we have iterated through biases from 20 TECU to 50 TECU in 0.1 TECU steps and shell heights from −700 km to 1800 km in 100 km steps. A lower shell height limit of −700 km was chosen, as the projection function becomes imaginary for some elevations if shell heights below this value are used. As one can see from this figure, there is a tendency for the surface to converge to a global minimum, but this minimum does not occur before running into the lower shell height limit. The minimum for this experiment occurs at the edge of the domain at 44.4 TECU for a shell height of −700 km. The question remains: why does this approach not work as one may expect?

While the MSD approach makes logical sense, it has never been tested in an environment that adheres to its unrealistic requirement for horizontal homogeneity, and thus, it is unknown how the method reacts to violations of its fundamental assumptions.

In Figure 6b, we have applied the cominimization MSD approach to a simulated, horizontally homogeneous environment above Resolute for a 24 h period on 1 July 2013, with a simulated bias of 5 TECU. The mean ionospheric shell height, calculated as the average shell height estimated through the CM shell height approach of equation (7), was 366.5 km for this experiment. The global minimum of Figure 6b corresponds to a bias of 5.0 TECU and a shell height of 360 km; thus, global minimum of the SSD surface corresponds

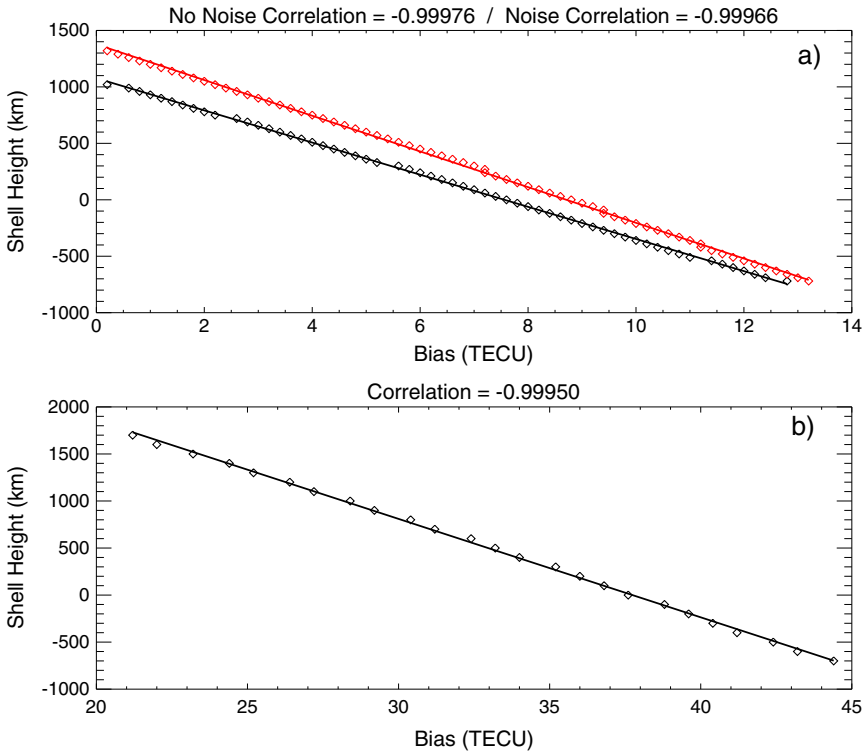

Figure 7. (top) The 1 TECU noise (red) and zero-noise (black) simulation MSD bias sensitivity at Resolute (diamonds) and corresponding fitted curves (solid lines) for 1 July 2013. (bottom) Same as top plot but for real GPS data at Resolute for 1 July 2013.

remarkably well to the true, simulated shell height and bias. In fact, this is the case for all simulations tested (every 24 h period available between January 2009 and January 2013) with a mean difference of 2.0 km and 0.1 TECU and standard deviations of 15 km in shell height and 0.2 TECU in bias, respectively. This shows that, in an environment that adheres to the assumptions required of the MSD approach, the cominimization method provides accurate shell height and bias values even while making the thin shell ionosphere assumption.

If we now add noise to the simulation, we arrive at behavior similar to that of the real GPS data. Figure 6c was generated using a 1.0 TECU standard deviation Gaussian noise for the same period as Figures 6a and 6b. It is clear from this example that the addition of even a modest amount of noise can result in the same type of unrealistic behavior exhibited using real GPS data, where the global minimum of the SSD surface was driven down toward lower shell heights and has taken on unrealistic and unphysical values (−330 km, 10.8 TECU), which do not correspond to the simulated truth. We may thus conclude that the use of a cominimization approach, while accurate in the absence of horizontal gradients, is not a viable option for bias and shell height estimation in real environments, at least not in the polar cap region. That said, simulations clearly show that it is possible to simultaneously extract bias and shell height information. Further research may indeed be able to make use of this information.

3.1.3. Shell Height

As detailed in the introduction to section 3, the MSD approach to receiver bias estimation requires the use of an ionospheric projection function and as such is subject to the limitations associated with the chosen projection method. In this and most other applications of the MSD method, we use the thin shell ionosphere assumption detailed section 2 and described by equation (2). This method requires that we select an altitude for the thin ionospheric layer. Several studies have attempted to identify the true ionospheric shell height through models and other approaches [*Komjathy and Langley*, 1996; *Birch et al*., 2002; *Mushini et al*., 2009], but few have attempted to identify the impact that the choice of shell height has on GPS receiver bias estimation [*Carrano and Groves*, 2006], and none have done so in a rigorous manner.

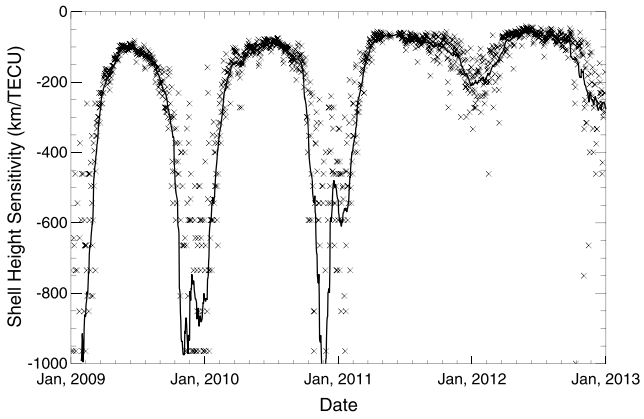

Figure 8. MSD bias sensitivity to shell height at Resolute for real GPS data between 2009 and 2013 (crosses) and superimposed 28 day smoothed bias sensitivity.

Let us first consider the sensitivity of the traditional MSD approach to errors in shell height. To assess this sensitivity, we simply calculate the MSD bias using a series of shell height values. An example of this is presented in Figure 7a, where we have used simulated data with and without noise and shell heights ranging between 0 km and 2000 km in 10 km steps. It is clear from this figure that the MSD bias is almost perfectly linearly dependent on the choice of shell height in the control environment; in fact, for all of the data tested, never does the linear Pearson's correlation between bias and shell height decrease below $R = 0.98$. The same calculation was done for real GPS data and is presented in Figure 7b. Again, the shell height and bias appear to be highly linearly correlated.

In Figure 8, we present the MSD sensitivity to shell height for the Resolute station for the same period used in Figure 5. MSD shell height sensitivity varies from extremely large values of several thousand kilometers per TECU in solar minimum winter to less than 50 km per TECU during solar maximum summer. This implies that even small, systematic biases in our choice of shell height can materialize as seasonal and solar cycle variabilities in the estimated bias. This is somewhat expected as the projection function is very nearly linear with shell height over the 0 km–2000 km range. Shell height sensitivity of bias estimation can thus be taken as linear, where the sensitivity variability is actually linearly dependent on the true mean sTEC; hence, the observed sensitivity variability trend of increased sensitivity during summer and high solar activity periods.

3.2. Least Squares

The LSQ approach to receiver bias estimation of *Lanyi and Roth* [1988] looks to identify a receiver bias value that removes the correlation between projected vTEC and the projection function. For this purpose, it uses a simple polynomial model to account for local ionospheric variability.

3.2.1. The Method

In the LSQ receiver bias estimation method, one models the ionospheric vTEC by a simple polynomial, such as the following:

$$\mathrm{vTEC} = a + b\theta + c\varphi + d\varphi\theta + e\theta^2 + f\varphi^2 \tag{8}$$

where a, b, c, d, e, and f are the fitting coefficients, θ is the latitude, and φ is the local time. The sTEC measured by the receiver can then be expressed as

$$\mathrm{sTEC} = \frac{\mathrm{vTEC}}{M(e)} + \mathrm{DCB} \tag{9}$$

where DCB refers to the receiver bias. By fitting GPS sTEC measurements to the above relationship by a linear regression, one can extract the expected receiver bias.

While typical applications of this technique use short integration periods (2–4 h), this application has been shown to result in highly erroneous and unstable biases for stations in the polar cap region [*Themens et al.*, 2013]. The high degree of horizontal inhomogeneity and variability of the polar cap ionosphere forces us to use longer integrations in this region to overcome some of these issues. For this study, we use 12 and 24 h integration periods. In Figure 9, biases are derived using the LSQ approach at the Resolute station for the same period displayed in Figure 5 using 24 and 12 h integrations for local nighttime and local daytime periods. We may note that the issues outlined in *Themens et al.* [2013] seem to be largely resolved through the use of these longer integration periods, as compared to the MSD biases presented in Figure 5. Comparing the three integration periods used, we see the same type of behavior as that between the integration periods of the MSD approach.

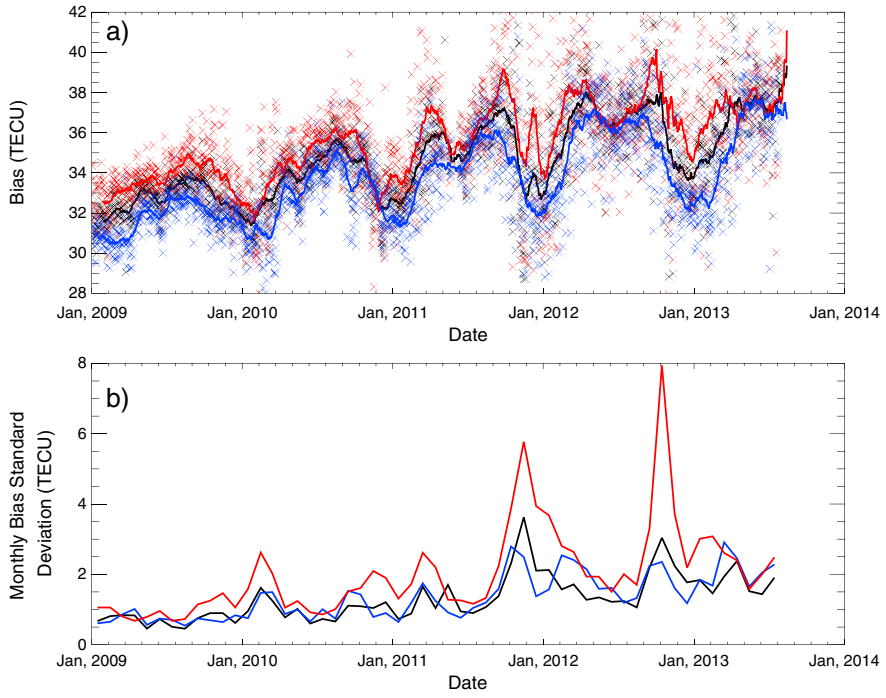

Figure 9. Same as Figure 5 but for the local time LSQ method.

3.2.2. The Effect of Coordinate System and Model Choice

It has been suggested that one should use a magnetic coordinate system for the LSQ method at high latitudes, as variability is often more strongly driven by magnetic convection than by photoionization in these regions, particularly during the solstices [*Lunt et al.*, 1999b; *Themens et al.*, 2013]. To determine the impact of our choice of coordinate system on LSQ bias estimation, we have determined receiver biases at the Resolute station using Altitude Adjustment-Corrected Geomagnetic Coordinates-derived magnetic latitude and magnetic local time in place of the corresponding geographic coordinates in equation (8). Figure 10a shows the biases derived using the magnetic LSQ approach for the Resolute station for the same period as Figure 5 for daytime and nighttime conditions. Figure 10b depicts the differences between nighttime magnetic and standard LSQ biases for the Resolute station. This figure shows that the use of a magnetic coordinate system generally leads to higher LSQ biases while using a 10° elevation cutoff, particularly during the winter and equinox periods. Using a 30° elevation cutoff, the use of a magnetic coordinate system generally results in lower estimated bias by between 0 and 2 TECU, peaking during the spring equinox.

3.3. Elevation Cutoff Sensitivity

As bias estimation methods attempt to determine biases through the removal of erroneous bias projections in the transformation between sTEC and vTEC, one may easily assert that the variation in elevation angle of satellites should have a significant impact on the technique's ability to identify what constitutes bias projection errors among violations of the technique's fundamental tenets, namely, horizontal homogeneity. In fact, we should expect that these techniques will break down as the variation in vTEC due to projected bias becomes hidden behind errors due to horizontal inhomogeneity and natural ionospheric variability; thus, the ability of a bias estimation technique to determine the receiver bias is dependent both on its ability to account for horizontal inhomogeneity and on the available variation in elevation angle. This feature is highlighted in the high-latitude region, where overhead observations are unavailable and ionospheric patches/arcs become troublesome sources of horizontal small-scale inhomogeneity. The station used in this study, Resolute, lies well within the polar cap region, where polar cap patches and travelling ionospheric disturbances are a regular occurrence and GPS satellites do not exceed 65° elevation angle [*MacDougall and Jayachandran*, 2007; *Jayachandran et al.*, 2012].

Past studies have often adopted a 30° elevation cutoff for bias estimation to avoid errors due to multipath errors in the projection function and to reduce the size of the region over which one must assume horizontal

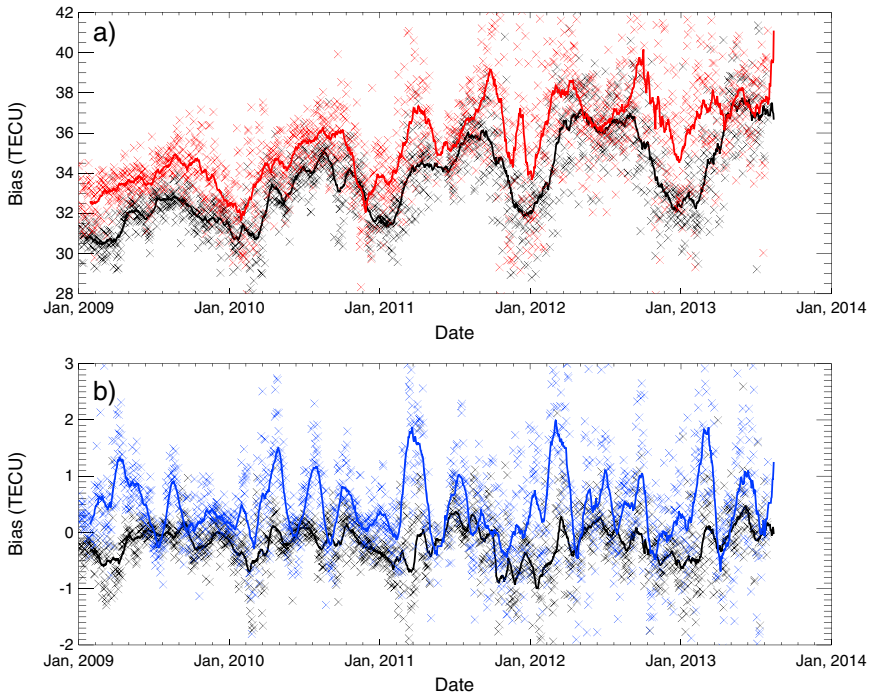

Figure 10. (top) Magnetic LSQ biases for daytime (red) and nighttime (black) integration periods at Resolute between 2009 and 2013. (bottom) Differences between local time and magnetic coordinate system-derived LSQ biases for nighttime using 10°cutoff (black) and 30° cutoff (blue). Positive values imply that local time LSQ biases are greater than the magnetic LSQ biases.

homogeneity [*Smith et al.*, 2008; *Themens et al.*, 2013]. While these are, of course, valid concerns, the implications of having less pronounced bias projection have not been addressed. To illustrate the effect of our selection of elevation cutoff, Figure 11 plots the differences between 10° and 30° cutoffs using the MSD and LSQ methods. From Figure 11, we may note that the use of a 30° elevation cutoff leads to lower biases than its 10° counterpart during select periods as solar activity increases. These differences are coincident with significant increases in geomagnetic activity. The 28 day smoothed sunspot number and summed daily *Ap* index are presented in Figure 12. This result is as we should expect, as increased geomagnetic activity is highly correlated with increased gradients and patches in the polar cap region [*MacDougall and Jayachandran*, 2007; *Jayachandran et al.*, 2012]. In these cases, any benefits from having a more pronounced bias projection are overcome by the increase in errors due to the increased horizontal inhomogeneity introduced through the use of a larger gathering area. In the case of the standard LSQ approach, 30° cutoff results are generally larger than their 10° counterpart, with the exception of the aforementioned periods of high geomagnetic activity. Magnetic LSQ sees comparable biases from both cutoff angles with the exception of periods of high geomagnetic activity. The 30° cutoff MSD biases are larger than 10° cutoff biases at solar minimum but quickly become comparable by 2011 and become lower than 10° cutoff biases during the equinox periods at solar maximum.

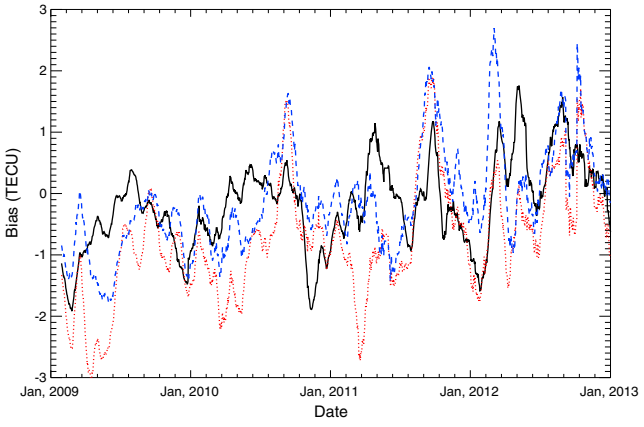

Figure 11. Differences between 10° cutoff and 30° cutoff biases for MSD (black), local time LSQ (red), and magnetic LSQ (blue) methods. Positive values imply that 10° cutoff biases are larger than 30° cutoff biases.

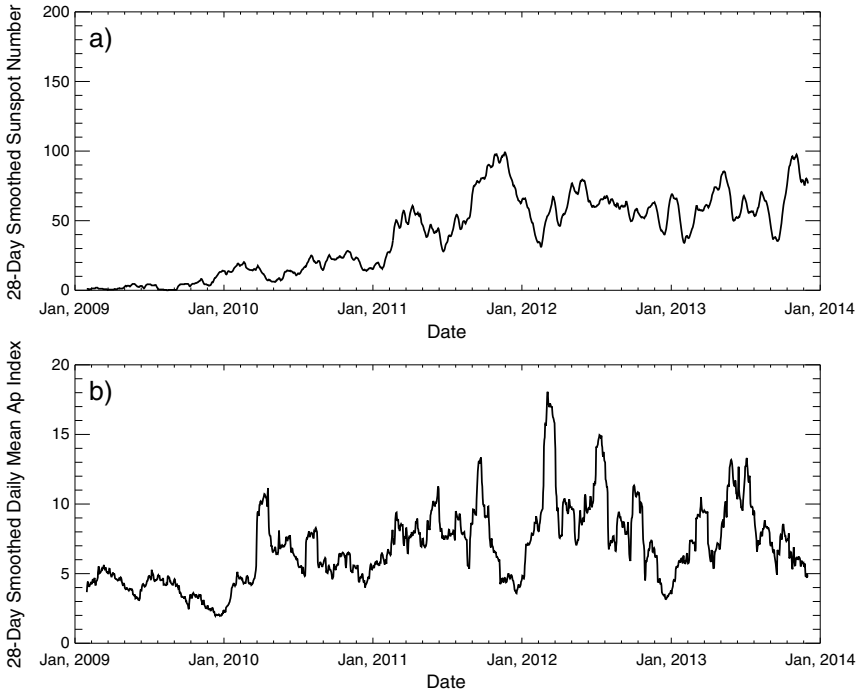

Figure 12. (top) The 28 day smoothed sunspot number. (bottom) The 28 day smoothed daily mean *Ap* index.

4. Results and Discussion

The biases presented in Figures 5, 9, and 10a all demonstrate strong seasonal and solar cycle variabilities. Correlating these biases to 28 day smoothed sunspot number results in linear Pearson's correlations of 0.567 for MSD, 0.554 for standard LSQ, and 0.568 for magnetic LSQ (all using a 10° elevation cutoff). It is unrealistic, however, to believe that receiver biases would truly vary with solar cycle, as the instrument hardware should have no reliance on the state of the ionosphere. *Coster et al.* [2013] have related bias variability to the site and outdoor temperature; however, as both tropospheric temperature and ionospheric variability have strong solar zenith angle dependencies, it is difficult to separate the effect of temperature on GPS biases from bias errors that result from ionospheric gradients or other ionospheric effects. Before one can conclusively determine the magnitude of a temperature dependence in GPS receiver biases, one must first either characterize the errors in current bias estimation methods, develop new bias estimation methods that do not rely on the use of the ionosphere, or conduct a direct comparison between GPS sTEC and that determined by a reference instrument. We will explore the first and third options.

The high-latitude environment and the instrument setup at Resolute together offer a unique opportunity to examine bias estimation errors and conduct a direct comparison between GPS and reference measurements. As will be discussed in section 4.3, in midlatitude regions one must make special consideration for plasmaspheric content when calculating GPS receiver biases. Also, ISRs are incapable of estimating electron density at plasmaspheric altitudes and thus cannot be used as a direct reference instrument for GPS bias estimation. These problems do not exist in the polar cap region, as plasmaspheric content in this region is largely nonexistent. This allows us to avoid having to consider the plasmasphere in this region.

In the following sections, we examine the effects of shell height choice, plasmaspheric content, temperature, and solar activity on both the true bias and bias estimation techniques.

4.1. Comparisons to Incoherent Scatter Radar

To examine the performance of these bias estimation techniques, we compare RISR-derived sTEC to that from the nearby CHAIN Resolute GPS. For this comparison, we simply project and integrate the ISR profiles to produce sTEC in the same manner as outlined in section 2.3. To insure that we are sampling a similar region from both instruments, we restrict GPS data to that which have a 400 km altitude IPP within the sampling

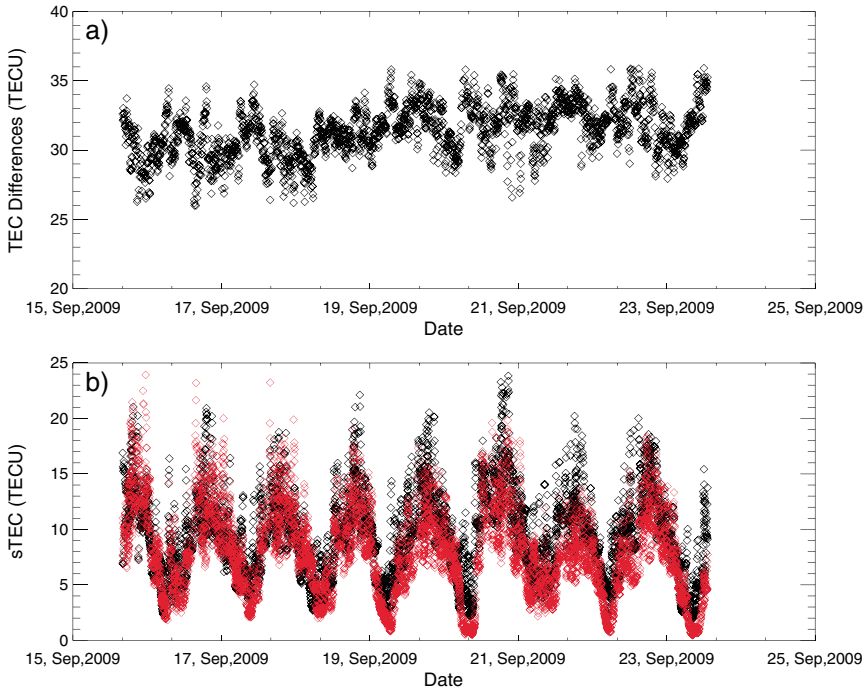

Figure 13. (top) GPS-ISR sTEC differences for 16–24 September 2009. (bottom) sTEC at Resolute from RISR-N (red) and GPS sTEC—30.0 TECU (black).

region of the RISR-N system. Once this is complete, we compare sTECs from both instruments, taking the median difference between the two as the expected receiver bias. An example of coincident GPS and RISR-N sTEC for 16–24 September 2009 is presented in Figure 13b, where GPS and RISR-N measurements demonstrate remarkably similar variability. In Figure 13a, we show the differences between GPS and ISR sTECs for the same period. One may note from this figure that the differences are largely stable over the course of the entire experiment.

For the sake of comparison with the LSQ and MSD biases, we present LSQ and MSD nighttime biases with experiment-averaged ISR-GPS differences in Figure 14. Total RMS differences between the various permutations of the MSD and LSQ bias estimation techniques and the ISR-derived biases are presented in Table 1 with monthly RMS errors plotted in Figure 15. From this table and figure we may finally make conclusions with regard to the best approach to apply these standard bias estimation methods. Based solely on overall RMS errors, we may conclude that the MSD approach performs better than either LSQ method, that 10° cutoff outperforms 30° cutoff for both the MSD and local time LSQ methods, and that the local time/geographic and magnetic coordinate systems do not demonstrate particularly appreciable differences. For a 10° cutoff, the local time coordinate system slightly, but consistently, outperforms the magnetic coordinate system. The opposite is true for the 30° cutoff, where the magnetic coordinate system consistently demonstrates lower monthly errors. This is consistent with the observations of section 3.2.2, as all methods demonstrated overestimation with respect to ISR-GPS sTEC differences.

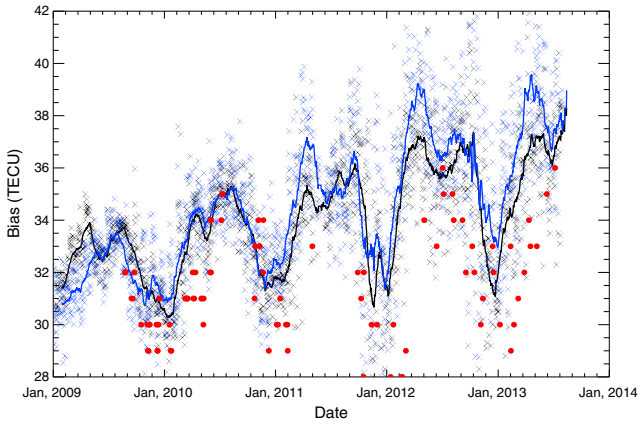

Figure 14. The 10° cutoff MSD (black) and local time (blue) biases at Resolute with experiment-averaged GPS-ISR sTEC differences (red). The solid lines represent 28 day smoothed biases.

Table 1. Total Receiver Bias Method RMS Errors

Method	Elevation Cutoff (Deg)	RMS Error (TECU)
MSD	10	2.68
MSD	30	2.83
MSD sunspot detrended	10	1.91
MSD sunspot detrended + temperature fit	10	1.66
LSQ-Mag	10	3.11
LSQ-Mag	30	3.04
LSQ-Loc	10	2.92
LSQ-Loc	30	3.37

Based on the RMS error results, we shall only consider 10° cutoff MSD in the remaining portion of this study.

One of the most striking features of Figure 14 is the fact that the GPS-ISR differences vary in a manner similar to that of the receiver bias estimation methods, particularly over seasonal time scales. This suggests that, somehow, the observed seasonal variabilities in the receiver bias are in fact real. The question remains, how is this possible and what is driving the remaining solar cycle variability in the bias estimates? To answer this, we break the problem down into its many parts and examine the individual mechanisms through which these bias estimates may vary.

4.2. Bias Variability From Shell Height Errors

The first, and most commonly addressed, mechanism is that associated with our assumption of a particular ionospheric shell height. Our use of the MSD and LSQ bias estimation methods has required that we select an assumed ionospheric height. As the ionosphere is not steady state and can vary on diurnal, seasonal, and solar cycle time scales, assuming a single, constant shell height is unrealistic.

The question remains: can the relatively small errors in shell height, demonstrated in Figure 3, account for the unrealistic solar cycle bias variability demonstrated by the MSD and LSQ methods? To answer this question, we use an estimate of true ionospheric shell height, derived from CADI electron density profiles using the CM approach, and examine the errors we should expect given our selection of a 400 km shell height in our bias estimation and the shell height sensitivities presented in Figure 8. Figure 16b presents the monthly median difference between the 10° cutoff MSD bias using the 400 km shell height and that calculated using the true shell height for all periods of available Resolute CADI data. Figure 16a shows the monthly median bias

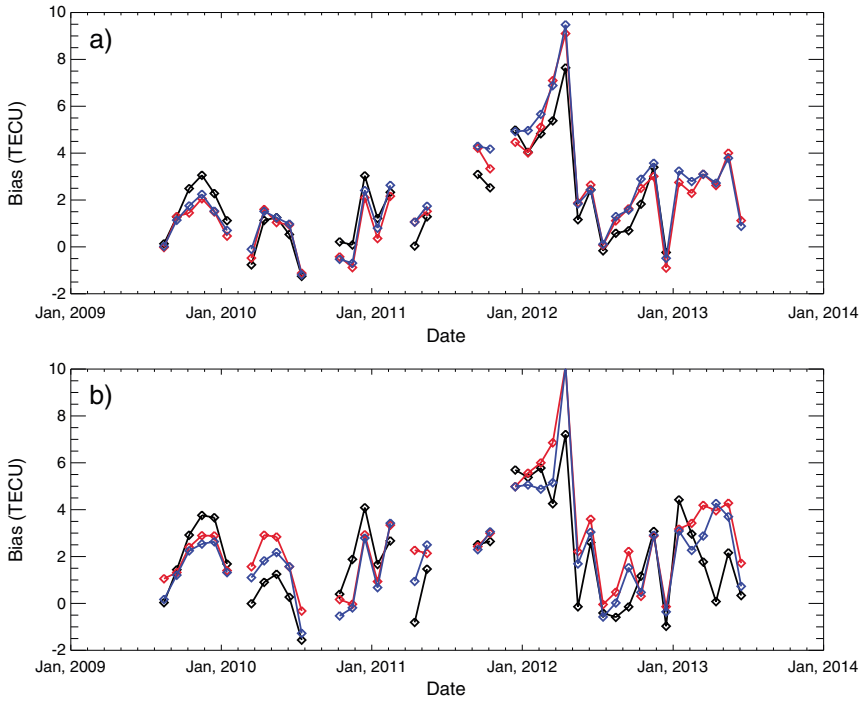

Figure 15. (top) Monthly averaged MSD (black), local time LSQ (red), and magnetic LSQ (blue) errors at Resolute with respect to ISR observations. Positive values imply overestimation of biases for 10° cutoff. (bottom) Same as top plot but for 30° cutoff.

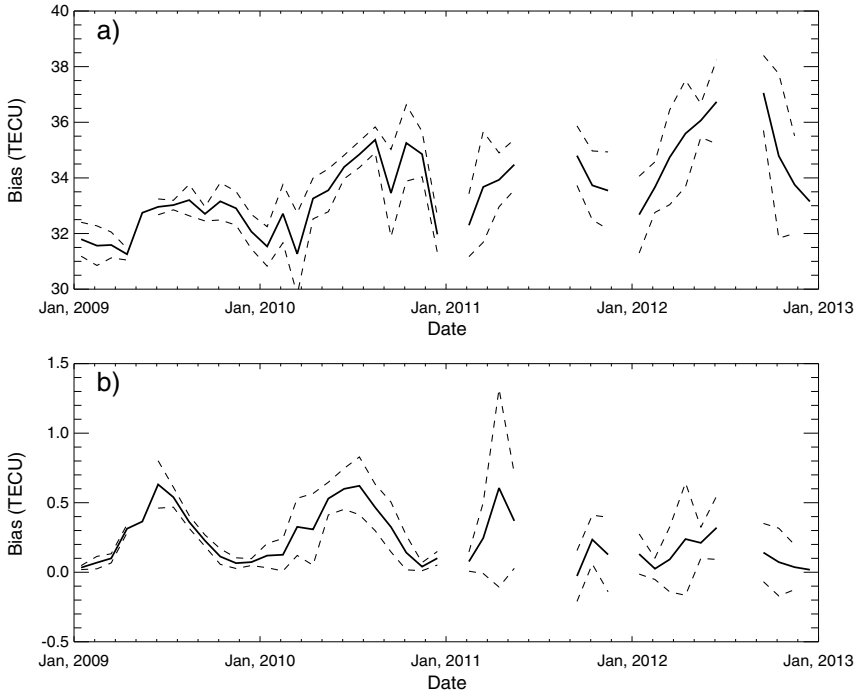

Figure 16. (top) Monthly median 10° cutoff MSD biases determined using CADI-derived shell height at Resolute (solid). Standard deviation error margins are also plotted (dashed). (bottom) Monthly median difference between 10° cutoff MSD biases calculated using 400 km and those calculated using CADI-derived shell heights. Positive values imply underestimation by the fixed 400 km shell height method.

determined by the 10° MSD approach using CADI-derived shell height. As you can see, the errors as a result of using the incorrect shell height do demonstrate seasonal and solar cycle variabilities but the magnitude of these errors is found to be less than 2 TECU, which, as is clear in Figure 16a, could not account for all of the observed solar cycle variabilities in these biases.

4.3. Plasmaspheric Electron Content

In all of the receiver bias estimation techniques presented, the bias is identified based on the assumption that it is the only geometrically free parameter contributing to the sTEC measurements (Tenet #3 of section 3). This assumption is not necessarily true, as plasmaspheric TEC (pTEC) can appear roughly geometry free to these methods; thus, if we project sTEC with an ionospheric projection function (400 km shell height), we would be significantly overestimating the geometric variability of the plasmaspheric contribution to the sTEC. With the addition of horizontal gradients and noise, this overprojection could easily be misinterpreted as bias by these methods.

To illustrate how pTEC is assimilated into the MSD-derived bias, we provide a simple example where we employ the same simulations as described in section 2.3 with the addition of a simple plasmaspheric layer beginning at 2000 km altitude. Table 2 presents the results of these simulations for a noise-free environment and various configurations of plasmasphere with a 5 TECU simulated bias. The CM of the full electron density profile is given in the third column, the bias estimated using a 400 km shell height is given in the fourth column, the percent of pTEC that is misinterpreted as bias by the estimation method is given in the fifth column, and the bias calculated using the CM as the shell height in bias estimation is given in the last column of Table 2.

The proportion of pTEC wrongly interpreted as bias in these methods varies between 70% and 80% for the simple simulations tested. One might be able to adjust for this error by increasing the projection shell height; however, as shown in Table 2 with the true CM height, the high degree of asymmetry in the profile results in new errors in estimated bias. This leaves operators of middle- and low-latitude stations with a significant challenge in their bias estimation, as pTEC can exceed 10 TECU at those locations [*Lunt et al.*, 1999a; *Mazzella*, 2009].

Table 2. Bias, Shell Height, and Plasmaspheric Contribution to Bias Using Simple Plasmasphere Simulations and 5 TECU Simulated Bias

Plasmaspheric Thickness (km)	pTEC (TECU)	CM (km)	Bias at 400 km (TECU)	% pTEC	Bias at CM (TECU)
Not applicable (NA)	0	374.31	4.71	NA	4.91
2000	1	489.02	5.45	74.10	4.74
2000	3	687.84	6.93	73.95	4.48
2000	5	855.20	8.40	73.88	4.29
4000	1	501.08	5.50	79.28	4.70
4000	3	725.51	7.08	79.11	4.35
4000	5	918.97	8.68	79.39	4.11

This mechanism has been extensively researched in the works of *Lunt et al*. [1999a, 1999b], *Mazzella et al*. [2002], and *Mazzella* [2009]. While this is a significant concern for midlatitude observations, the absence of an appreciable plasmasphere in the polar cap region [*Lunt et al*., 1999a; *Nsumei et al*., 2008] debunks this as a mechanism through which the observed biases, and thus the ISR-GPS comparisons, should vary at the Resolute site. This appears to leave only true receiver bias variability as an explanation for the observed GPS-ISR sTEC differences presented in Figure 14. Recent studies suggest temperature as the main driver for this variability [*Rieck et al*., 2003; *Ciraolo et al*., 2007; *Coster et al*., 2013].

4.4. Temperature

Using the direct ISR-GPS sTEC comparisons, we attempt to assess the potential for a receiver bias temperature dependence. For this purpose, we have linearly least squares fitted ISR-GPS sTEC differences to hourly temperature measurements made at the nearby (within 5 km) Resolute Environment Canada Climate Weather Station (74.72°N, 265.02°E), taken as an approximate measure of the outdoor temperature at the GPS station (climate data can be accessed at http://climate.weather.gc.ca/). The linear Pearson's correlation between ISR-GPS differences and outdoor temperature is found to be 0.311 (57,018 data points) and is plotted in Figure 17. The slope of this fit is found to be 0.1154 ± 0.0015 TECU/°C, resulting in a seasonal bias variability of ~5 TECU annually. This result is statistically significant and is comparable to the results of *Coster et al*. [2013]. The remaining spread in the fit is likely the result of small-scale patches that may be observed by one measurement system without the other, simply due to the slight differences in sampling area, particularly during the daytime. It should be noted that the receiver unit itself is kept in a temperature-controlled environment, implying that the observed temperature variability in bias is likely the result of temperature-dependent dispersion in the outdoor cabling and antenna.

This is an encouraging result, suggesting that the observed seasonal bias variability is in fact real and can be predictable. This, of course, leaves us with the problem of nonnegligible differences between ISR-calculated and method-estimated biases, as shown in Figure 15, associated with solar cycle variability and seasonal variations in ionospheric gradients. In order for standard receiver bias estimation methods to provide accurate bias estimates at high latitudes, we must identify a means to account for these differences.

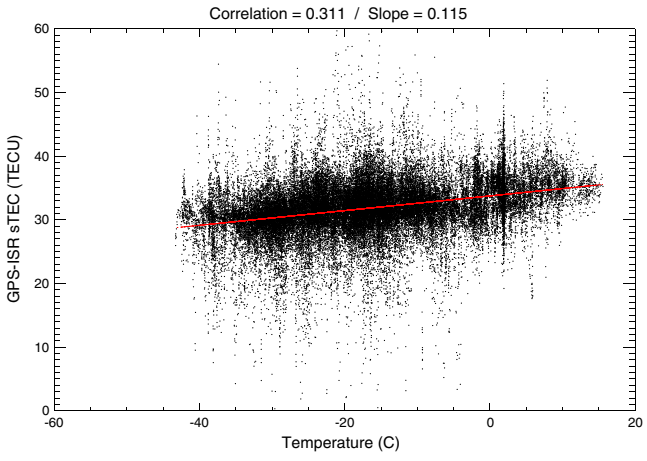

Figure 17. Comparison between GPS-ISR sTEC differences and hourly outdoor temperature at Resolute with least squares fit superimposed (red).

4.5. Solar Activity

We have here observed a general tendency for the MSD and LSQ bias estimation methods to overestimate the receiver bias, particularly as solar activity increases. This tendency for bias overestimation is likely the result of large-scale ionospheric gradients. As the Resolute station is located near the geographic and geomagnetic poles, TEC often increases in all directions

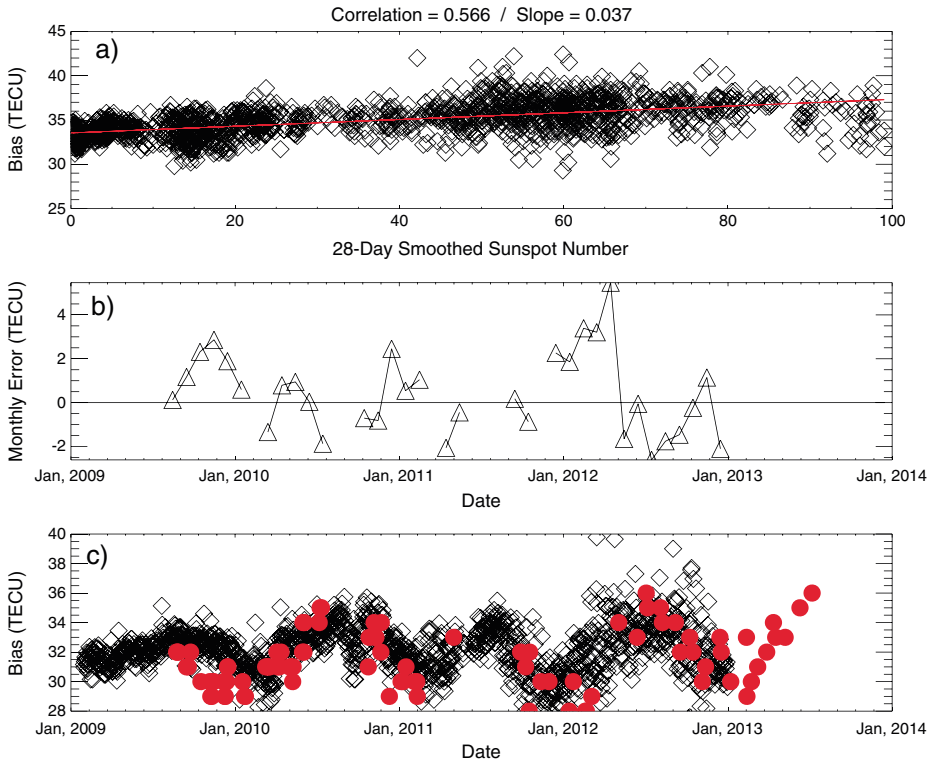

Figure 18. (top) Fit of 10° cutoff MSD bias to 28 day smoothed sunspot number. (middle) Monthly averaged errors between GPS-ISR sTEC differences and 10° cutoff MSD after the sunspot variability in bias has been removed. (bottom) Sunspot-detrended 10° cutoff MSD bias (black) and GPS-ISR sTEC differences (red).

away from the station. This tendency means that not only should sTEC decrease with increasing elevation angle due to the geometry of the raypath but also because of the natural, large-scale ionospheric gradients. These gradients can appear correlated with the geometric projection function and thus may be misinterpreted as bias projection by bias estimation methods. The effect of these large-scale ionospheric gradients on bias estimation in the polar cap will be addressed in future work; however, middle- and low-latitude studies, such as *Ciraolo et al.* [2007], *Mazzella* [2009], *Brunini and Azpilicueta* [2010], and *Conte et al.* [2011], already show that ionospheric gradients can materialize as seasonal and solar cycle bias variations in standard receiver bias estimation methods.

Regardless of the mechanism through which these errors propagate into bias estimates, a method must be developed to remove these errors before these standard bias estimation approaches can be applied accurately in the region. For this purpose, we have linear least squares fitted the MSD-derived biases to 28 day smoothed sunspot number. This fit is presented in Figure 18a with linear Pearson's correlation coefficient and slope listed in the header of the plot. We can then remove this correlation from the bias estimates. The sunspot-detrended biases are presented in Figure 18c. As you can see, these corrected biases represent a significant improvement and match ISR-derived biases reasonably well. The monthly average differences between these corrected biases and ISR-derived biases are presented in Figure 18b. As you can see, errors are generally less than 2 TECU and the previous ~7 TECU error in spring 2012 has been reduced to ~5 TECU.

There are still appreciable errors during the equinoxes, particularly in early 2012. These errors can likely be attributed to an abrupt increase in geomagnetic activity during these periods, seen in Figure 12, as well as to the tendency for ionospheric gradients to steepen at high latitudes during the equinoxes. To accommodate these errors, one can simply avoid the application of these bias methods during periods of high geomagnetic activity ($Ap > 20$). One can then fit the remaining sunspot-detrended bias to the site temperature and use this fit to interpolate the bias for these periods. An example of this process is presented in Figure 19a, where only winter (December, January, and February) and summer (June, July, and August) periods with daily mean

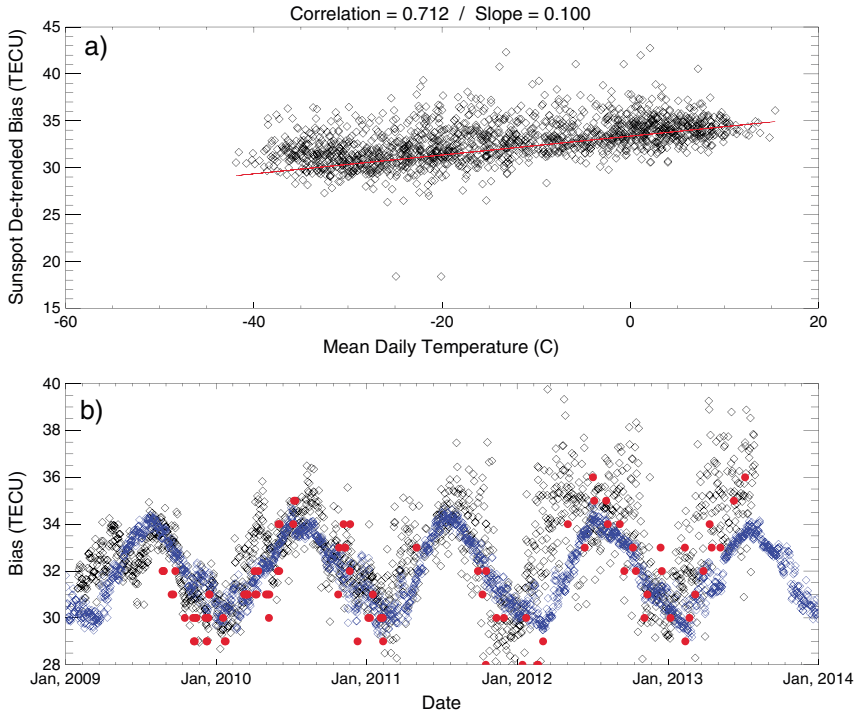

Figure 19. (top) Fit of sunspot detrended, 10° cutoff MSD bias, and mean daily outdoor temperature at Resolute. (bottom) Sunspot detrended, 10° cutoff MSD bias (black), bias from temperature fitting (blue), and GPS-ISR sTEC differences (red) at Resolute.

Ap index less than 10 were used in the fit to daily mean temperature. The fit demonstrates a linear Pearson's correlation of 0.712 (446 data points) and a slope of 0.100 ± 0.005 TECU/°C, comparable to that observed using GPS-ISR sTEC differences. The resulting interpolated biases are presented in Figure 19b, and total RMS errors from ISR observations are found to be 1.66 TECU. This marks an appreciable improvement over the traditional application of the MSD method, as the equinox issues in bias estimation are corrected. This method of fitting and interpolation also fixes the issue of bias instability, which can become significant as solar activity increases. This is illustrated in Figures 5b and 9b, where we have presented the monthly standard deviation of MSD and LSQ biases, respectively. The caveat to both sunspot and temperature fitting, however, is the requirement for long (several years) bias records without hardware changes. This is not a realistic requirement for some system deployments.

5. Conclusions

In this study, we have examined the behavior of standard, single-station, receiver bias estimation methods with respect to violations of their fundamental assumptions. These assumptions are necessarily violated in real ionospheric environments, particularly at high and equatorial latitudes; thus, it is important to understand and account for the effects of these violations, particularly when we are seeing unrealistic solar cycle variability in estimated receiver biases.

We first examined the effect of shell height on bias estimation, finding that bias sensitivity to shell height is locally linear and varies seasonally and with solar cycle. Despite this linear relationship, it is found that, under ideal circumstances, it is possible to determine shell height and bias simultaneously; however, these ideal circumstances are not experienced in real ionospheric systems. Future research may yet be able to decouple bias and shell height in real applications. We next examined the behavior of the LSQ bias estimation method using local time and magnetic coordinate systems. While using a 10° elevation cutoff, local time LSQ biases during winter periods are consistently lower than those found using the magnetic coordinate system. Using a 30° elevation cutoff results in lower biases by the magnetic LSQ method, particularly during periods of high geomagnetic activity.

As we are interested in the high-latitude region, where satellite elevations rarely exceed ~60°, the choice of elevation cutoff can have significant implications for the bias estimation. The 10° cutoff biases tend to be lower than those from their 30° counterpart during winter periods for MSD and spring for local time LSQ. All methods produce lower biases using 10° cutoffs during solar minimum but transition to producing larger biases as solar and geomagnetic activity increases.

To evaluate the performance of these various bias estimation methods, and their permutations, we have undertaken a direct comparison to ISR observations. At midlatitudes this would not be possible as plasmaspheric content cannot be observed by the ISR system. In the polar cap, however, plasmaspheric content is largely negligible. Using this comparison, we find that 10° cutoff MSD biases outperform the other bias methods/permutations tested. Using MSD and local LSQ, 10° cutoffs outperform 30° cutoffs. Over the period tested, local LSQ is found to outperform magnetic LSQ. Comparing GPS- and ISR-derived sTECs, we find that GPS biases do in fact demonstrate real seasonal, but not solar cycle, variability. These ISR-derived biases are found to correlate well with outdoor temperature at the site tested, likely due to temperature-dependent dispersion in the cabling and antenna hardware. We find that the erroneous solar cycle variability in estimated biases cannot be explained solely by shell height variability but rather likely results from large-scale ionospheric gradients correlated with the vertical projection function. To account for these errors we find that simply correlating estimated biases to 28 day smoothed sunspot number and removing the trend results in a significant improvement in method performance. If we then assume that true bias variability is only driven by temperature changes, we can then fit the sunspot-detrended biases to temperature to again improve the performance and stability of bias estimation. While these measures constitute a significant improvement in bias estimation performance, they require long (several years) periods over which to undertake the sunspot and temperature correlations, making these adjustments impossible to achieve in short-term deployment situations.

Acknowledgments

RISR-N is operated by SRI on behalf of the U.S. National Science Foundation (NSF) under NSF Cooperative Agreement AGS-1133009. Infrastructure funding for CHAIN was provided by the Canada Foundation for Innovation and the New Brunswick Innovation Foundation. CHAIN operations are conducted in collaboration with the Canadian Space Agency. Science funding is provided by the Natural Sciences and Engineering Research Council of Canada. Ionosonde and GPS data are available from the CHAIN website at http://chain.physics.unb.ca/chain/. Incoherent scatter radar data are available from the SRI International Database at http://amisr.com/database/ or from the Madrigal Database at http://isr.sri.com/madrigal/. The authors would like to thank Michael Nicolls of SRI International for his assistance in the processing the incoherent scatter radar data.

Michael Balikhin thanks Knut Jacobsen and Thomas Gaussiran II for their assistance in evaluating this paper.

References

Arikan, F., H. Nayir, U. Sezen, and O. Arikan (2008), Estimation of single station interfrequency receiver bias using GPS-TEC, *Radio Sci.*, *43*, RS4004, doi:10.1029/2007RS003785.

Bahcivan, H., R. T. Tsunoda, M. J. Nicolls, and C. J. Heinselman (2010), Initial ionospheric observations made by the new Resolute Incoherent Scatter Radar and comparison to solar wind IMF, *Geophys. Res. Lett.*, *37*, L15103, doi:10.1029/2010GL043632.

Birch, M. J., J. K. Hargreaves, and G. J. Bailey (2002), On the use of an effective ionospheric height in electron content measurement by GPS reception, *Radio Sci.*, *37*(1), doi:10.1029/2000RS002601.

Brunini, C., and F. Azpilicueta (2010), GPS slant total electron content accuracy using the single layer model under different geomagnetic regions and ionospheric conditions, *J. Geod.*, *84*(5), 293–304.

Carrano C. S., and K. M. Groves (2006), The GPS segment of the AFRL-SCINDA Global Network and the Challenges of Real-Time TEC Estimation in the Equatorial Ionosphere, Proceedings of ION NTM 2006, Monterey, Calif., 18–20 Jan.

Ciraolo, L., F. Azpilicueta, C. Brunini, A. Meza, and S. M. Radicella (2007), Calibration errors on experimental slant total electron content (TEC) determined with GPS, *J. Geod.*, *81*, 111–120, doi:10.1007/S00190-006-0093-1.

Coïsson, P., S. M. Radicalle, R. Leitinger, and B. Nava (2006), Topside electron density in IRI and NeQuick: Features and limitations, *Adv. Space Res.*, *37*, 937–942.

Conte, J. F., F. Azpilicueta, and C. Brunini (2011), Accuracy assessment of the GPS-TEC calibration constants by means of a simulation technique, *J. Geod.*, *85*(10), 707–714.

Coster, A., J. Williams, A. Weatherwax, W. Rideout, and D. Herne (2013), Accuracy of GPS total electron content: GPS receiver bias temperature dependence, *Radio Sci.*, *48*, 190–196, doi:10.1002/rds.20011.

Davies, K. (1990), *Ionospheric Radio*, *IEE Electromagn. Waves Ser.*, vol. 31, Peter Peregrinus, Stevenage, U. K.

Dyrud, L., A. Jovancevic, A. Brown, D. Wilson, and S. Ganguly (2008), Ionospheric measurement with GPS: Receiver techniques and methods, *Radio Sci.*, *43*, RS6002, doi:10.1029/2007RS003770.

Evans, J. (1969), Theory and practice of ionosphere study by Thomson scatter radar, *Proc. IEEE*, *57*(4), 496–530.

Gaussiran, T., D. Munton, B. Harris, and B. Tolman (2004), An open source toolkit for GPS processing, total electron content effects, measurements and modeling, in *Proceedings of the International Beacon Symposium*, Trieste, Italy.

Jayachandran, P. T., et al. (2009), Canadian High Arctic Ionospheric Network (CHAIN), *Radio Sci.*, *44*, RS0A03, doi:10.1029/2008RS004046.

Jayachandran, P. T., K. Hosokawa, K. Shiokawa, Y. Otsuka, C. Watson, S. C. Mushini, J. W. MacDougall, P. Prikryl, R. Chadwick, and T. D. Kelly (2012), GPS total electron content variations associated with poleward moving Sun-aligned arcs, *J. Geophys. Res.*, *117*, A12311, doi:10.1029/2009JA014216.

Keshin, M. (2012), A new algorithm for single receiver DCB estimation using IGS TEC maps, *GPS Solut.*, *16*(3), 283–292.

Komjathy, A., and R. Langley (1996), Improvement of a global ionospheric model to provide ionospheric range error corrections for single-frequency GPS users, in *Proceedings of the 52nd Annual Meeting of the Institute of Navigation*, pp. 557–566, Cambridge, Mass., 22–24 Jan.

Lanyi, G. E., and T. Roth (1988), A comparison of mapped and measured total ionospheric electron content using Global Positioning System and beacon satellite observations, *Radio Sci.*, *23*, 483–492, doi:10.1029/RS023i004p00483.

Leick, A. (2004), *GPS Satellite Surveying*, 3rd ed., John Wiley, Hoboken, N. J.

Lunt, N., L. Kersley, and G. J. Bailey (1999a), The influence of the protonosphere on GPS observations: Model simulations, *Radio Sci.*, *34*(3), 725–732, doi:10.1029/1999RS900002.

Lunt, N., L. Kersley, G. J. Bishop, A. J. Mazzella, and G. J. Bailey (1999b), The effect of the protonosphere on the estimation of GPS total electron content: Validation using model simulations, *Radio Sci.*, *34*(5), 1261–1271, doi:10.1029/1999RS900043.

Ma, G., and T. Maruyama (2003), Derivation of TEC and estimation of instrumental biases from GEONET in Japan, *Ann. Geophys.*, *21*, 2083–2093.

Ma, X. F., T. Maruyama, G. Ma, and T. Takeda (2005), Determination of GPS receiver differential biases by neural network parameter estimation method, *Radio Sci.*, *40*, RS1002, doi:10.1029/2004RS003072.

MacDougall, J., and P. T. Jayachandran (2007), Polar patches: Auroral zone precipitation effects, *J. Geophys. Res.*, *112*, A05312, doi:10.1029/2006JA011930.

Mazzella, A. J., Jr. (2009), Plasmasphere effects for GPS TEC measurements in North America, *Radio Sci.*, *44*, RS5014, doi:10.1029/2009RS004186.

Mazzella, A. J., E. A. Holland, A. M. Andreasen, C. C. Andreasen, G. S. Rao, and G. J. Bishop (2002), Autonomous estimation of plasmasphere content using GPS measurements, *Radio Sci.*, *37*(6), 1092, doi:10.1029/2001RS002520.

Mushini, S. C., P. T. Jayachandran, R. B. Langley, and J. W. MacDougall (2009), Use of varying shell heights derived from ionosonde data in calculating vertical total electron content (TEC) using GPS—New method, *J. Adv. Space Res.*, *44*, 1309–1313, doi:10.1016/j.asr.2009.07.015.

Nsumei, P. A., B. W. Reinisch, P. Song, J. Tu, and X. Huang (2008), Polar cap electron density distribution from IMAGE radio plasma imager measurements: Empirical model with the effects of solar illumination and geomagnetic activity, *J. Geophys. Res.*, *113*, A01217, doi:10.1029/2007JA012566.

Petrie, E. J., M. Hernández-Pajares, P. Spalla, P. Moore, and M. King (2011), Review of higher order ionospheric refraction effects on dual frequency GPS, *Surv. Geophys.*, *32*, 197–253.

Rideout, W., and A. Coster (2006), Automated GPS processing for global total electron content data, *GPS Solut.*, doi:10.1007/s10291-006-0029-5.

Rieck, C., P. Jarlemark, K. Jaldehag, and J. Johansson (2003), Thermal influence on the receiver chain of GPS carrier phase equipment for time and frequency transfer, in *Proceedings of the 2003 IEEE International Frequency Control Symposium*, Tampa, Fla.

Smith, D. A., E. A. Araujo-Pradere, C. Minter, and T. Fuller-Rowell (2008), A comprehensive evaluation of the errors inherent in the use of a two-dimensional shell for modeling the ionosphere, *Radio Sci.*, *43*, RS6008, doi:10.1029/2007RS003769.

Themens, D. R., P. T. Jayachandran, R. B. Langley, J. W. MacDougall, and M. J. Nicolls (2013), Determining receiver biases in GPS-derived total electron content in the auroral oval and polar cap region using ionosonde measurements, *GPS Solut.*, *17*(3), 357–369, doi:10.1007/s10291-012-0284-6.

Themens, D. R., P. T. Jayachandran, M. J. Nicolls, and J. W. MacDougall (2014), A top to bottom evaluation of IRI 2007 within the polar cap, *J. Geophys. Res. Space Physics*, *119*, 6689–6703, doi:10.1002/2014JA020052.

Titheridge, J. E. (1985), Ionogram analysis: Least squares fitting of a Chapman layer peak, *Radio Sci.*, *20*(2), 247–256, doi:10.1029/RS020i002p00247.

Titheridge, J. E. (1988), The real height analysis of ionograms: A generalized formulation, *Radio Sci.*, *23*(5), 831–849, doi:10.1029/RS023i005p00831.

Warnant, R. (1997), Reliability of the TEC computed using GPS measurements—The problem of hardware biases, *Acta Geod. Geophys. Hung.*, *32*(3–4), 451–459.

Zhang, D. H., W. Zhang, Q. Li, L. Q. Shi, Y. Q. Hao, and Z. Xiao (2010), Accuracy analysis of the GPS instrumental bias estimated from observations in middle and low latitudes, *Ann. Geophys.*, *28*(8), 1571–1580.

Zhang, W., D. H. Zhang, and Z. Xiao (2009), The influence of geomagnetic storms on the estimation of GPS instrumental biases, *Ann. Geophys.*, *27*(4), 1613–1623.